Interaction of a Contact Resonance of Microspheres with Surface Acoustic Waves

N. Boechler,[1] J. K. Eliason,[2] A. Kumar,[1] A. A. Maznev,[2] K. A. Nelson,[2] and N. Fang[1]

[1]*Department of Mechanical Engineering, Massachusetts Institute of Technology, Cambridge, Massachusetts 02139, USA*

[2]*Department of Chemistry, Massachusetts Institute of Technology, Cambridge, Massachusetts 02139, USA*

(Received 1 March 2013; revised manuscript received 11 June 2013; published 17 July 2013)

We study the interaction of surface acoustic waves (SAWs) with a contact-based vibrational resonance of 1 μm silica microspheres forming a two-dimensional granular crystal adhered to a substrate. The laser-induced transient grating technique is used to excite SAWs and measure their dispersion. The measured dispersion curves exhibit ''avoided crossing'' behavior due to the hybridization of the SAWs with the microsphere resonance. We compare the measured dispersion curves with those predicted by our analytical model and find excellent agreement. The approach presented can be used to study the contact mechanics and adhesion of micro- and nanoparticles as well as the dynamics of microscale granular crystals.

DOI: 10.1103/PhysRevLett.111.036103 PACS numbers: 68.35.Iv, 45.70.−n, 46.55.+d, 78.47.jj

Wave phenomena in granular media is a rich and rapidly developing field of research [1–3]. At the heart of this field is the Hertzian model of elastic contact between spherical particles, in which the stiffness of the contact depends on the applied force [4]. One type of granular media, often referred to as ''granular crystals,'' consists of close-packed, ordered arrays of elastic particles that interact via Hertzian contact [2,3]. Granular crystals have been shown to support a wide range of linear and nonlinear dynamical phenomena not encountered in conventional materials and have been suggested for various engineering applications [2,3].

Acoustic studies of granular media typically involve macroscopic particles with dimensions of ~0.1–10 mm [1–3], whereas contact-based vibrations of microparticles with dimensions of (or under) ~1 μm remain largely unexplored. The scale factor is significant as a microparticle system cannot be thought of simply as a scaled-down version of a macroscale system which is governed by the same physics. Rather, microparticles are expected to yield qualitatively different dynamics. One crucial factor is adhesion [5,6], which is almost negligible on millimeter scales but significant on micron scales. Because of adhesion, a microsphere in contact with a substrate is pulled toward the latter. This results in an equilibrium contact area and ''contact resonances'' with vibration frequencies determined by the particle mass, the adhesion, and the elastic properties of the particle and substrate [7–10]. This phenomenon has been observed experimentally in microspheres for rocking [7], axial [8], and lateral [9,10] vibrations. Eigenmodes corresponding to free-particle vibrations have also been observed at much higher frequencies [11].

In this Letter, we study a contact resonance of microspheres forming a two-dimensional granular crystal adhered to a substrate using a hitherto unexplored phenomenon, i.e., the interaction of contact resonances of microparticles with surface acoustic waves (SAWs) in the substrate. We use the laser-induced transient grating (TG) technique [12,13] to excite long-wavelength (relative to the particle size) SAWs and measure their dispersion. The measured dispersion curves exhibit classic ''avoided crossing'' [14] behavior due to the hybridization of the SAWs with the contact resonance of microspheres. Such coupling between SAWs and mechanical surface oscillators was studied in the theoretical works [15–17] and the experimental work [18]. We analyze our measurements using a simple model that assumes an axial contact resonance and yields an analytical expression for the dispersion relation. We find excellent agreement between our model and the measurements using the frequency of the contact resonance as a single fitting parameter, and we compare our results with estimates based on the Derjaguin-Muller-Toporov (DMT) contact model [19].

Our sample is a hexagonally packed monolayer of $D = 1.08$ μm diameter silica microspheres deposited on an aluminum-coated fused silica substrate, as shown in Figs. 1(b) and 1(c). The silica slab is 1.5 mm thick, and

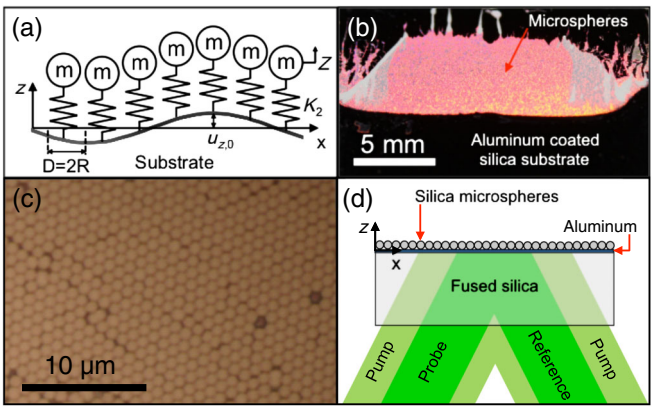

FIG. 1 (color online). (a) Microspheres interacting with a SAW via contact ''springs,'' with notations used in the theoretical model. (b) Photograph of the sample. (c) Representative image of the silica microsphere monolayer. (d) Schematic illustration of the TG setup.

the aluminum, which serves as a medium to absorb pump laser light, is 0.20 μm thick. To assemble the monolayer on the substrate, we used the "wedge-shaped cell" convective self-assembly technique [20–22]. The resulting monolayer has an area of ~5 mm × 10 mm, as shown in Fig. 1(b). A representative optical image of the monolayer packing is shown in Fig. 1(c). Although the monolayer has a uniform distribution, defects and grains of uniform packing are clearly present.

We use a laser-induced TG technique [12,13] to measure the phase velocity dispersion of SAWs in our sample. The TG setup used for these experiments has been described previously [13]. In summary, two excitation beams derived from the same laser source (515 nm wavelength, 60 ps pulse duration, 2.44 μJ total pulse energy at the sample) enter the sample through the silica substrate, as shown in Fig. 1(d), and are overlapped at the aluminum layer forming a spatially periodic interference pattern. The pump spot has 500 μm diameter at $1/e^2$ intensity level. Absorption of the laser light by the aluminum film induces rapid thermal expansion, which leads to the generation of counterpropagating SAWs with wavelength λ_S defined by the period of the interference pattern. The period is controlled by a phase mask pattern used to create the two excitation beams by splitting the incident beam into $+/-1$ diffraction orders [12]. Switching phase mask patterns allows measurements at multiple acoustic wavelengths.

SAW detection is accomplished using a quasi-cw probe beam (532 nm wavelength, 10.7 mW average power at the sample) focused at the center of the excitation pattern to a spot of 150 μm diameter. The probe beam also enters the sample through the silica substrate and is diffracted by surface ripples and refractive index variations in the substrate induced by SAWs [23]. The diffracted beam is overlapped with the reflected reference beam (local oscillator) [12,13] and directed onto a fast avalanche photodiode with a 1 GHz bandwidth. The signal is recorded using an oscilloscope and averaged over 10^4 repetitions.

Figures 2(a) and 2(b) show typical signals acquired at an acoustic wave vector magnitude $k = 2\pi/\lambda_S = 0.46\ \mu\text{m}^{-1}$. Figure 2(a) shows the signal from a sample location without microspheres, and Fig. 2(b) corresponds to a location with spheres. In both cases there is a sharp initial increase, which corresponds to the excitation pulse arriving at the sample. The slowly decaying component is due to the "thermal grating" associated with the temperature profile in the sample [12,13]. The high frequency oscillations are due to acoustic waves.

Figures 2(c) and 2(d) show the Fourier spectra of acoustic oscillations corresponding to the signals in Figs. 2(a) and 2(b) [22]. In the off-spheres case there are two clear peaks, which correspond to a Rayleigh SAW (the low frequency peak) and a longitudinal wave in the substrate [24]. Figure 3 shows the acoustic dispersion curves. For the off-spheres case, we see linear dispersion curves that agree

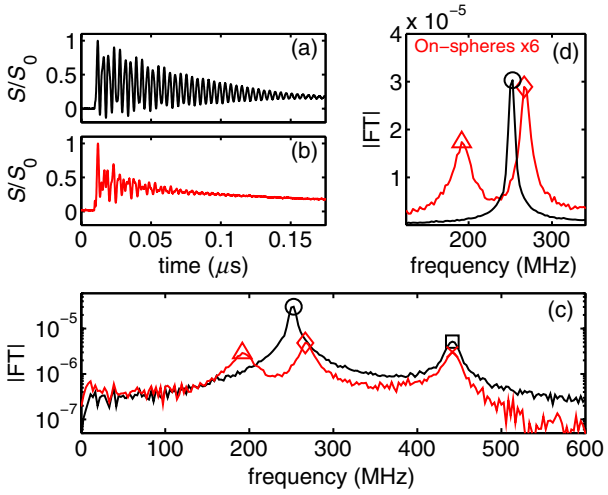

FIG. 2 (color online). Normalized signal (a) off-spheres and (b) on-spheres for $k = 0.46\ \mu\text{m}^{-1}$. The acquired signal S is normalized by the maximum signal amplitude S_0. Fourier transform (FT) magnitudes corresponding to the signals in (a) and (b) plotted in log scale (c) and linear scale (d). The black curve corresponds to the signal in (a), and the red curve to the signal in (b). The markers denote the identified peaks, which are plotted in Fig. 3 using the same markers.

well with lines corresponding to the longitudinal and Rayleigh wave velocities in fused silica. We used typical wave speeds for fused silica of $c_L = 5968$ m/s (longitudinal) and $c_T = 3764$ m/s (transverse) [25], and calculated the Rayleigh wave velocity $c_R = 3409$ m/s by numerically solving the Rayleigh equation [26]. More accurate calculations accounting for the aluminum layer

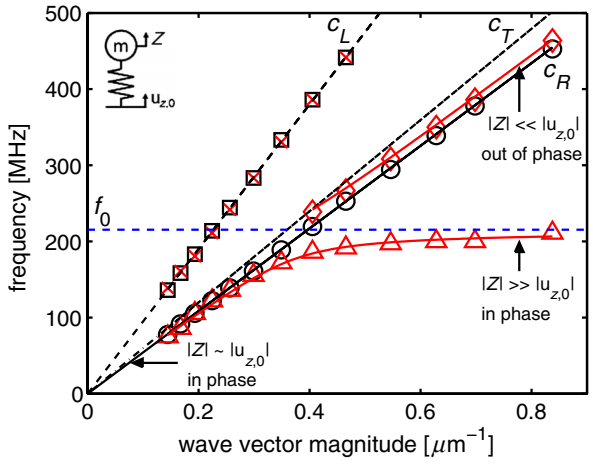

FIG. 3 (color online). Dispersion relations. Red and black markers are the measured frequency peaks for the on- and off-spheres cases, respectively. The solid red line is the dispersion calculated using our model. Also shown are lines corresponding to longitudinal, transverse, and Rayleigh waves in fused silica, and a horizontal line corresponding to the microsphere contact resonance frequency.

[22,26] showed that the reduction in the Rayleigh wave velocity due to the aluminum layer does not exceed 1.4%.

The on-spheres case yields starkly different behavior from the off-spheres case, as can be seen by comparing the signals in Figs. 2(a) and 2(b). The comparison of the spectra in Fig. 2(c) shows that the longitudinal peak is unaffected by the presence of the spheres whereas the SAW peak is split in two. The on-spheres dispersion curves in Fig. 3 reveal a classic "avoided crossing" between the Rayleigh wave and a local microsphere resonance. The lower branch starts as a Rayleigh wave at low wave vector magnitudes and approaches a horizontal asymptote corresponding to the resonance frequency. The upper branch is close to the Rayleigh wave at high wave vector magnitudes; in the "avoided crossing" region it deviates from the Rayleigh line and stops at the threshold corresponding to the transverse acoustic velocity of the substrate.

To describe SAW propagation in our system of microspheres coupled to an elastic substrate, we adapt an approach developed in the theoretical works [15–17]. As shown schematically in Fig. 1(a), we model the substrate as an elastic half-space ($z \leq 0$), where the surface of the half-space is connected to an array of linear surface oscillators, with mass m and linearized normal contact stiffness K_2, which represent the microspheres connected to the substrate via axial "contact springs." We calculate the microsphere mass m using a density of $\rho_s = 2.0$ g/cm^3 as provided by the manufacturer (Corpuscular, Inc.).

We approximate the microspheres as point masses, as the lowest spheroidal resonance of the microspheres $f_2 = 3.1$ GHz [27] is much greater than the frequencies observed in the experiment. The equation of motion for the surface oscillator can be written as $m\ddot{Z} + K_2(Z - u_{z,0}) = 0$, where $u_{z,0}$ is the displacement of the substrate surface, and Z is the displacement of the oscillator relative to the surface. The particles exert a vertical force on the substrate, leading to the following boundary conditions at the surface $z = 0$:

$$\sigma_{zz} = \frac{K_2(Z - u_{z,0})}{A} \qquad \sigma_{xz} = 0, \tag{1}$$

where σ_{zz} and σ_{xz} are components of the elastic stress tensor [26], and $A = (\sqrt{3}D^2/2)$ is the area of a primitive unit cell in our hexagonally packed monolayer.

Since the acoustic wavelength is much larger than the sphere size, in Eq. (1) we use an effective medium approach and approximate the average normal stress at the surface as the force exerted by the microsphere "spring" divided by the area of a unit cell. We follow the standard procedure for the derivation of the Rayleigh wave equation [26] but use Eq. (1) instead of stress-free boundary conditions to obtain the following dispersion relation for the SAWs in our coupled oscillator system [22]:

$$\left(\frac{\omega^2}{\omega_0^2} - 1\right)\left[\left(2 - \frac{\omega^2}{k^2 c_T^2}\right)^2 - 4\left(1 - \frac{\omega^2}{k^2 c_L^2}\right)^{1/2}\left(1 - \frac{\omega^2}{k^2 c_T^2}\right)^{1/2}\right] = \frac{m}{A\rho_2}\frac{\omega^4(1 - \frac{\omega^2}{k^2 c_L^2})^{1/2}}{k^3 c_T^4}, \tag{2}$$

where $\omega_0 = 2\pi f_0 = \sqrt{K_2/m}$ is the angular frequency of the contact resonance, and $\rho_2 = 2.2$ g/cm^3 [28] is the density of the silica substrate. On the left-hand side of Eq. (2), the term in square brackets is familiar from the Rayleigh equation, and the term in the parentheses describes the resonance of the oscillators. The right-hand side of Eq. (2) is responsible for the coupling between the Rayleigh waves and the oscillators; if it is made to vanish (for instance, by assuming a vanishing areal density m/A), then the oscillators and SAWs in the substrate are effectively decoupled. We also see that A and ρ_2 relate to the coupling strength, K_2 relates to the frequency of the avoided crossing through ω_0, and m relates to both.

By taking the frequency of the contact resonance as a fitting parameter and using least squares minimization between the numerical solution of Eq. (2) and the measured dispersion, we find $f_0 = 215$ MHz. The fitted resonant frequency is plotted as the blue dashed line in Fig. 3 and gives a contact stiffness of $K_2 = 2.4$ kN/m. We plot the numerical dispersion curve from our fitting as the red solid line in Fig. 3.

Any real solution of Eq. (2) must yield the phase velocity ω/k smaller than c_T, otherwise, at least one of the square root terms becomes imaginary. Therefore, the calculated upper dispersion branch terminates at the threshold $\omega = c_T k$, in agreement with the experiment. In some cases, leaky wave solutions with complex ω can be found above the threshold [17]; however, we did not investigate complex solutions since in our experiment the upper branch peak disappeared past the threshold.

Using the oscillator equation of motion, we estimated the relative displacements (and phase) of the microspheres and the surface for various limiting cases [22], as is shown in Fig. 3. In the flat dispersion region of the lower branch, there is predominantly sphere oscillation with very small surface displacements. Indeed, our experimental data show that the amplitude of the corresponding peak becomes progressively smaller compared to the Rayleigh-like upper branch as the wave vector magnitude is increased [22]. This is supported by measurements taken from the front side, which show the opposite trend due to signal contributions from the spheres [22]. Because of our detection mechanism, the dominance of lower branch in the front-side measurements also suggests that we are observing sphere motion normal to the surface.

We estimate the frequency of the axial contact resonance (and the contact stiffness) of the microspheres using the DMT contact model [19,22] and compare with the resonant frequency obtained from the measured data. The DMT model describes the contact between an elastic sphere

and a flat substrate under the presence of adhesive forces. For small displacements, the full DMT model can be approximated as [19]

$$F = KR^{1/2}\alpha^{3/2} - 2\pi wR, \tag{3}$$

where F is a force applied to the sphere, α is the displacement of the center of the sphere towards the substrate, $w = 0.094$ J/m^2 is the work of adhesion between silica and alumina (as the aluminum surface is normally oxidized) [22], R is the effective microsphere radius of contact ($R = D/2$ for a sphere on a flat substrate [4]), and $K = [(3/4)(((1-\nu_s^2)/E_s) + ((1-\nu_1^2)/E_1))]^{-1}$ is the effective modulus, where the aluminum has elastic modulus $E_1 = 62$ GPa and Poisson's ratio $\nu_1 = 0.24$ [29], and the microspheres have elastic modulus $E_s = 73$ GPa and Poisson's ratio $\nu_s = 0.17$ [30]. Using Eq. (3), we calculate the equilibrium displacement $\alpha_0 = (2\pi wR^{1/2}/K)^{2/3} = 0.44$ nm, the linearized stiffness around the equilibrium point $K_{2,\mathrm{DMT}} = (3/2)(2\pi wR^2K^2)^{1/3} = 1.1$ kN/m, and $f_{0,\mathrm{DMT}} = (1/2\pi)\sqrt{K_{2,\mathrm{DMT}}/m} = 140$ MHz. Below the axial contact resonance, a lateral mode is also predicted $f_l = ((R\alpha_0)^{1/4}/\pi m^{1/2})(((2-\upsilon_s)(1+\upsilon_s)/E_s) + ((2-\upsilon_1)(1+\upsilon_1)/E_1))^{-1/2}$ [10], where for our parameters $f_l = 0.9 f_{0,\mathrm{DMT}}$; however, front-side measurements suggest out-of-plane sphere motion. A rocking mode is also predicted $f_{\mathrm{rock}} = (1/2\pi)(1/R^{3/2})\sqrt{45w/4\rho_s} = 9.1$ MHz [7]; however, this is significantly below our measured acoustic frequency range. The discrepancy between the estimated and the measured values of f_0 may be caused by uncertainties in the contact and adhesion models. For instance, a greater work of adhesion than predicted could result in higher contact stiffnesses and resonant frequencies. We note that the work of adhesion can be determined from the measured resonant frequency using a contact model. Challenges in application of DMT to real nanoscale contacts have been underscored by studies in atomic force microscopy [5,31]. Typical adhesion studies relying on measuring a pull-off force provide limited information for verification of adhesion theories [5,7]. Our experiment provides a direct pathway to the contact stiffness, and thus offers a promising tool for studying adhesion and contact mechanics.

Comparing the on- and of-spheres cases, we see broader peaks in Fig. 2(d) and faster acoustic signal decay in Fig. 2(a) for the on-spheres case. In the off-spheres case, the acoustic signal decays as the SAW wave packet leaves the probe spot [32]. In the on-spheres case, the group velocity is lower, yet the decay time is shorter, which indicates additional attenuation. One possible mechanism is scattering due to the spheres. A single oscillator on a half-space will radiate energy into the substrate while a collective mode of a periodic array with $\omega < c_T k$ will not [17,32]. In our case, disorder may lead to scattering and radiation into the bulk. In the flat region of the lower dispersion branch, the peak width may also be determined by inhomogeneous broadening caused by sphere-to-sphere contact stiffness variation. Peak broadening may also be caused by anharmonicity, but we estimate sphere displacements in the linear regime [22], and no anharmonic effects are observed.

We have seen that an avoided crossing between the Rayleigh wave and contact resonance of the spheres occurs at wavelengths much larger than the size of the unit cell and is well described by the effective medium approximation. Thus, our structure belongs to a class of "locally resonant metamaterials" for which interesting effects have been observed on the macroscale [33,34]. We expect the effective medium model to break down at shorter wavelengths where phononic crystal effects should be seen [35]. Furthermore, our model treats the spheres as independent oscillators that interact through the elastic substrate but not directly. Although the spheres are close-packed, the model describes the data well. We believe that this is, again, due to the fact that the acoustic wavelength is large compared to the size of the unit cell [15]. At shorter wavelengths we expect to see rich dynamics due to interaction between the spheres [36,37].

In summary, we have studied the interaction of SAWs with a contact-based resonance of microspheres forming a two-dimensional granular crystal. The experimental method can be used to study the adhesion and contact mechanics of microparticles. It also enables the study of granular crystals on the microscale. A rich array of dynamical phenomena observed in macroscale granular crystals and their promise for practical applications [3] suggest interesting possibilities for microscale granular crystals. An analogy can also be made between SAWs interacting with a microsphere contact resonance and surface plasmon-polariton waves in a metal film interacting with a localized surface plasmon resonance of a nearby metallic nanoparticle [38]. This may lead to acoustic analogies of some plasmonic phenomena and applications [39]. Finally, the nonlinearity of the Hertzian contact holds promise for an application of our approach to developing nonlinear SAW devices.

N. B. thanks G. Theocharis and J. Xu for useful discussions and K. Broderick for guidance in substrate fabrication. This work was supported by the Defense Threat Reduction Agency through Grant No. HDTRA 1-12-1-0008. A. K. and N. X. F. are also partially supported by NSF Grant No. CMMI-1120724.

[1] H. Hinrichsen and D. E. Wolf, *The Physics of Granular Media* (Wiley-VCH Verlag GmbH & Co. KGaA, Weinheim, 2004).

[2] V. F. Nesterenko, *Dynamics of Heterogeneous Materials* (Springer-Verlag, New York, 2001).

[3] G. Theocharis, N. Boechler, and C. Daraio, in *Acoustic Metamaterials and Phononic Crystals*, edited by P. A. Deymier (Springer, Berlin, 2013), Vol. 173, Chap. 7.
[4] H. Hertz, J. Reine Angew. Math. **92**, 156 (1882).
[5] B. Bhushan, *Handbook of Micro/Nano Tribology* (CRC Press, Boca Raton, FL, 1999), 2nd ed.
[6] J. Israelachvili, *Intermolecular and Surface Forces* (Elsevier, Inc., Burlington, MA, 2011).
[7] M. D. Murthy Peri and C. Cetinkaya, J. Colloid Interface Sci. **288**, 432 (2005).
[8] Y. Guillet, B. Audoin, M. Ferrie, and S. Ravaine, Phys. Rev. B **86**, 035456 (2012).
[9] G. L. Dybwad, J. Appl. Phys. **58**, 2789 (1985).
[10] E. Vittorias, M. Kappl, H. J. Butt, and D. Johannsmann, Powder Technol. **203**, 489 (2010).
[11] T. Dehoux *et al.*, Opt. Lett. **34**, 3740 (2009).
[12] J. A. Rogers, A. A. Maznev, M. J. Banet, and K. A. Nelson, Annu. Rev. Mater. Sci. **30**, 117 (2000).
[13] J. A. Johnson, A. A. Maznev, M. T. Bulsara, E. A. Fitzgerald, T. C. Harman, S. Calawa, C. J. Vineis, G. Turner, and K. A. Nelson, J. Appl. Phys. **111**, 023503 (2012).
[14] J. von Neumann and E. Wigner, Phys. Z. **30**, 465 (1929).
[15] Y. A. Kosevich and E. S. Syrkin, Phys. Lett. **135A**, 298 (1989).
[16] A. R. Baghai-Wadji, V. P. Plessky, and A. V. Simonian, Sov. Phys. Acoust. **38**, 442 (1992).
[17] E. A. Garova, A. A. Maradudin, and A. P. Mayer, Phys. Rev. B **59**, 13291 (1999).
[18] Y. Achaoui, A. Khelif, S. Benchabane, L. Robert, and V. Laude, Phys. Rev. B **83**, 104201 (2011).
[19] V. M. Muller, B. V. Derjaguin, and Y. P. Toporov, Colloids Surf. **7**, 251 (1983); M. D. Pashley, Colloids Surf. **12**, 69 (1984).
[20] J. Sun, C.-J. Tang, P. Zhan, Z.-L. Han, Z.-S. Cao, and Z.-L. Wang, Langmuir **26**, 7859 (2010).
[21] V. Canalejas-Tejero, M. Ibisate, D. Golmayo, A. Blanco, and C. López, Langmuir **28**, 161 (2012).
[22] See Supplemental Material at http://link.aps.org/supplemental/10.1103/PhysRevLett.111.036103 for additional details.
[23] By comparing with measurements made from the front side (opposite from the silica substrate), we find that the signal contribution from surface ripples is dominant, except for longitudinal waves, where the refractive index contribution is dominant.
[24] Strictly speaking, a bulk longitudinal wave does not propagate along the free surface. However, there is an evanescent disturbance that propagates with the longitudinal wave velocity, see A. G. Every and G. A. D. Briggs, Phys. Rev. B **58**, 1601 (1998).
[25] D. R. Lide, *Handbook of Chemistry and Physics* (CRC Press, Boca Raton, FL, 2003).
[26] W. M. Ewing, W. S. Jardetzky, and F. Press, *Elastic Waves in Layered Media* (McGraw-Hill, New York, 1957).
[27] Y. Sato and T. Usami, Geophysical Magazine **31**, 15 (1962).
[28] D. E. Dieter, *Materials Selection and Design*, ASM Handbook Vol. 20 (ASM International, Materials Park, OH, 1997).
[29] ASM International Handbook Committee, *Properties and Selection: Nonferrous Alloys and Special-Purpose Alloys*, ASM Handbook Vol. 2 (ASM International, Materials Park, OH, 1990).
[30] N. P. Bansat and R. H. Doremus, *Handbook of Glass Properties* (Academic Press, Orlando, FL, 1986).
[31] M. Kopycinska-Muller, R. H. Geiss, and D. C. Hurley, Ultramicroscopy **106**, 466 (2006).
[32] A. A. Maznev and O. B. Wright, J. Appl. Phys. **105**, 123530 (2009).
[33] Z. Liu *et al.*, Science **289**, 1734 (2000).
[34] F. Lemoult, M. Fink, and G. Lerosey, Phys. Rev. Lett. **107**, 064301 (2011).
[35] H. R. Garner and T. Ohkawa, IEEE Trans. Ultrason. Ferroelectr. Freq. Control **40**, 69 (1993).
[36] Recent results indicate contact-based modes in nanosphere clusters, see M. Mattarelli, M. Montagna, T. Still, D. Schneider, and G. Fytas, Soft Matter **8**, 4235 (2012).
[37] V. Tournat, I. Pèrez-Arjona, A. Merkel, V. Sanchez-Morcillo, and V. Gusev, New J. Phys. **13**, 073042 (2011).
[38] J. J. Mock, R. T. Hill, Y.-J. Tsai, A. Chilkoti, and D. R. Smith, Nano Lett. **12**, 1757 (2012).
[39] S. A. Maier, *Plasmonics: Fundamentals and Applications* (Springer, New York, 2007).